Aging of Braze Joints: Interface Reactions in Base Metal/Filler Metal Couples, Part II: High-Temperature Au-Ni-Ti Braze Alloy

An examination of the effects of aging in brazed joints made with 81Au-17.5Ni-1.5Ti filler metal and Thermo-Span™ or AISI Type 347 stainless steel base metals revealed excellent wetting and spreading

BY P. T. VIANCO, F. M. HOSKING, J. J. STEPHENS, C. A. WALKER, M. K. NEILSEN, S. J. GLASS, AND S. L. MONROE

ABSTRACT. The effects of aging were examined in brazed joints made with 81Au-17.5Ni-1.5Ti filler metal and Thermo-Span™ or AISI Type 347 stainless steel base metals. Excellent wetting and spreading were observed with both base metals. The Thermo-Span/Au-Ni-Ti and AISI Type 347 stainless steel/Au-Ni-Ti joints exhibited an interdiffusion zone at the base metal/filler metal interfaces. Aging caused the interfacial diffusion zone to grow. Four-point bend strength tests and microstructural analysis identified a phase precipitation mechanism that maximized the joint strength when aged at 460°C.

Introduction

Engineered ceramics, such as silicon nitride (Si_3N_4) and partially stabilized zirconia (PSZ), have the physical and mechanical properties that allow their potential use in reciprocating and turbine engine systems (Refs. 1–3). Because metal alloy parts will still comprise a majority of heat engine components, there is a need for joining techniques of three categories: 1) metal-to-metal, 2) ceramic-to-ceramic, and 3) metal-to-ceramic.

The mechanical performance of any braze joint depends upon its microstructure. There are three critical regions in the brazed joint structure: 1) the filler metal, 2) the interface(s) between the filler metal and the base material, and 3) the base material(s). The initial microstructure of the brazed joint depends upon the base material and filler metal compositions as well as the brazing process parameters (Refs. 4–6). Exposure of the joint to prolonged

time periods at elevated temperature can cause solid-state reactions to occur in the filler metal, base materials, and at the interfaces. In particular, the development of interface reaction products can significantly alter the performance of the brazed joint.

The aging of brazed joints under long-term, elevated temperature exposure has not been extensively studied. Shimoo et al. studied the kinetics of solid-state reactions between Si_3N_4 and Ni (Ref. 7). Most aging studies have examined the interface microstructure that develops initially between the molten filler metal and the base material during the brazing process (Refs. 8–10).

An investigation was conducted to study the metal/metal interactions that occur within the joints made between two filler metals and two base metals. This report (Part II) examines the aging between a Au-Ni-Ti filler metal and the two base metals Thermo-Span™ and an AISI Type 347 stainless steel. (A prior study examined the aging of brazed joints made with a Ag-Cu-Ti filler metal and Thermo-Span or Inconel® 718 base metals; those results were reported as Part I.) Analytical tools were used to characterize the joint microstructures; four-point bend tests were used to determine the effect of microstructural changes on the mechanical performance of the joint.

KEY WORDS

Brazing
Brazement
Ceramic
Inconel®
Thermo-Span™
Aging
Precipitation Strengthening

Experimental Procedures

Materials – Base Metals

The two base metals and nominal compositions (wt-%) used in this study were 1) Thermo-Span, 24.5Ni-29.0Co-5.5Cr-4.8Nb-(Si, Ti, Al)-bal. Fe (Ref. 11) and 2) AISI Type 347 stainless steel, 18Cr-11Ni-2Mn-1Si-(Ta, Nb)-0.08C-bal. Fe. Thermo-Span is a precipitation-hardened alloy received in the solution-annealed condition (1093°C, 1 h, air cool). To ensure consistent material properties, the Thermo-Span was exposed to a precipitation-annealing heat treatment. The precipitation-hardened condition was confirmed through Rockwell-C (HR_C) hardness measurements. Six measurements were performed on three bare metal blanks. The heat treatment schedules and hardness data are presented below.

Thermo-Span (as-received HR_C = 23 ± 2, solution annealed):
Solution annealing (at the mill): 1093°C (2000°F) for 1 h; air cool.
Precipitation annealing: 718°C (1324°F) for 8 h; furnace cool at 0.015°C/s (0.027°F/s) to 621°C(1150°F); hold at 621°C for 8 h; air cooling.
Post-heat treatment HR_C = 39±1

All brazing experiments were performed on base metal specimens, the surfaces of which were ground to a nominal √32 finish. Profilometer traces determined the exact roughness as an arithmetic average roughness (RA) number. Four measurements were made, two in one direction and the other two in a perpendicular direction, over a distance of 6 mm. The mean and ± one standard deviation RA data are shown in Table 1. The solution and aging heat treatment given to the Thermo-Span resulted in a significant

P. T. VIANCO (ptvianc@sandia.gov), F. M. HOSKING, J. J. STEPHENS, C. A. WALKER, M. K. NEILSEN, S. J. GLASS, and S. L. MONROE are with Sandia National Laboratories, Albuquerque, N.Mex.
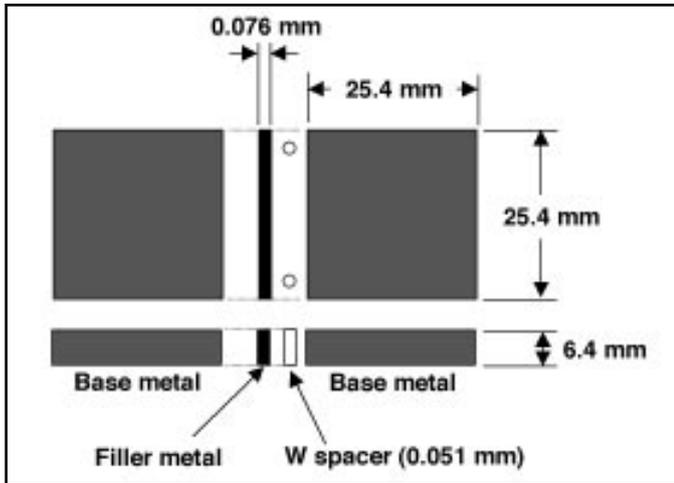
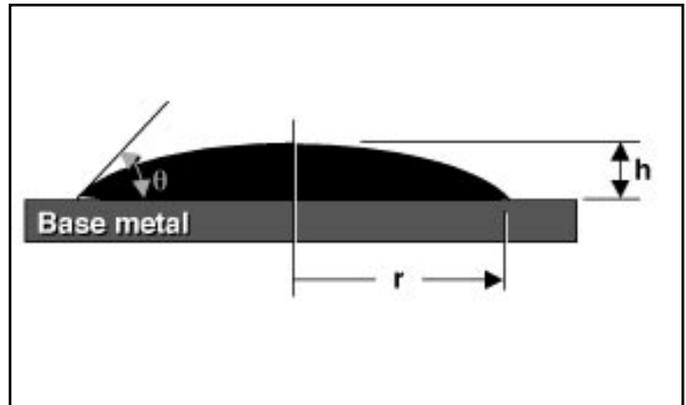*Fig. 1 — Assembly configurations for the metal/metal test samples.*

Fig. 2 — Schematic diagram of the sessile drop configuration used to assess the wettability of the braze alloys. The quantitative metric is the contact angle, θ. The symbol "r" is the effective spread radius assuming a circular footprint, and "h" is the height of the filler metal mound.

Table 1 — Arithmetic Average Roughness (RA) of the Metallic Test Samples with a √32 Finish Surface Profilometry Data (Med. Scan Speed)

Test Material	Condition	RA (μm)
Thermo-Span™	Solution treated	0.19 ± 0.02
Thermo-Span	Solution treated and aged	0.09 ± 0.02
347 stainless steel	As-received	0.03 ± 0.01

reduction in surface roughness after grinding as compared to that of the as-received material. The roughness of the AISI Type 347 stainless steel surface was similar to that of the aged Thermo-Span alloy.

Materials – Brazing Filler Metals

The filler metal was Wilbraze™ 81172R (Ref. 12). This material had a nominal composition of 81Au-17.5Ni-1.5Ti (wt-%). The baseline composition was 82Au-18Ni (T_{melt} = 955°C). Titanium was added (largely at the expense of the nickel component) to form an active braze alloy (ABA). Two batches of material were used in the study, one having a foil thickness of 0.051 mm (0.002 in.) and the other having a 0.025-mm (0.001-in.) foil thickness. Atomic emission spectroscopy (AES) was used to confirm the compositions of both material batches. The composition of the 0.051-mm-thick (0.001-in.) stock was 81.0 ± 1.2Au, 17.6 ± 0.1Ni, and 1.9Ti. The composition of the 0.025-mm-thick (0.002-in.) foil was 80.9 ± 5.6Au, 16.8 ± 0.7Ni, and 1.9Ti. The Au-Ni-Ti material had a cited melting range of 990 to 1020°C (1814 to 1868°F). The solidus temperatures, recorded by an in-house differential thermal analysis (DTA) study, were identical for both foils at 957°C (1755°F).

Parent Block, Brazed Joint Assembly

The test specimen configuration used

to evaluate the brazed joint microstructures, and from which the mechanical strength test pieces were fabricated, is shown in Fig. 1. The "parent" block of each base metal measured 25.4 x 25.4 x 6.4 mm (1.0 x 1.0 x 0.25 in.). Two blocks were joined along the 25.4 x 6.4 mm (1.0 x 0.25 in.) face, which had been ground to a nominal √32 finish. A piece of filler metal measuring 25.4 x 6.4 mm (1.0 x 0.25 in.) was placed between the two block surfaces. The joint clearance was controlled by the placement of two 0.051-mm-diameter (0.002-in.) tungsten wires in the joint clearance. The parent blocks, tungsten wires, and filler metal foil were stacked within a graphite fixture that maintained their alignment during the brazing process. A nominal mass was placed on top of the stack to ensure formation of the desired joint clearance.

Brazing Process

An extensive development effort was conducted to determine suitable brazing process parameters. First, an assessment was made of the variations in brazing temperature and time on wetting and joint microstructure. The nominal peak temperature was 1040°C (1904°F). The nominal peak time was 3 min. The brazing cycle was performed under a vacuum of 6.7 to 11 x 10^{-5} Pa (5 to 8 x 10^{-7} Torr) measured at the brazing temperature. The resulting mean and ± one standard deviation for the process temperature and time period
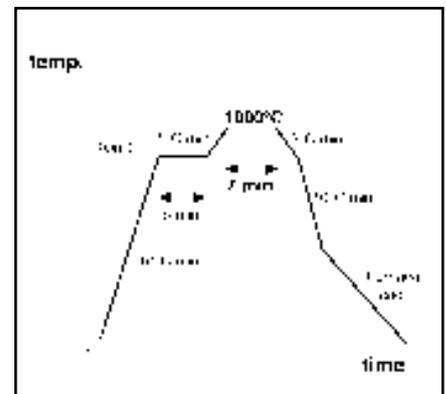

Fig. 3 — Time and temperature parameters for the Au-Ni-Ti brazing process.

following five furnace cycles were 1047±5°C (1917±9°F) and 2.0±0.3 min, respectively. The remainder of each temperature-time profile showed similarly good run-to-run consistency.

Sessile drop (area-of-spread) experiments assessed the filler metal wetting-and-spreading behavior as a function of brazing temperature and time. A filler metal preform was placed on the surface of each base material. The specimens were then exposed to one of the brazing cycles. The quantitative metric was the contact angle, θ, that formed at the droplet front — Fig. 2. The value of θ was calculated from the volume, V, of filler metal used to make the drop; an effective radius, r, of the footprint area; and the assumption the sessile drops were in the form of a spherical cap having a height, h. The value of h was calculated by Equation 1:

$$h = \{[(3V/\pi)2 + r6]1/2 + 3V/\pi\}1/3 -\{[(3V/\pi)2 + r6]1/2 - 3V/\pi\}1/3 \quad (1)$$

The contact angle was then calculated by equation 2:

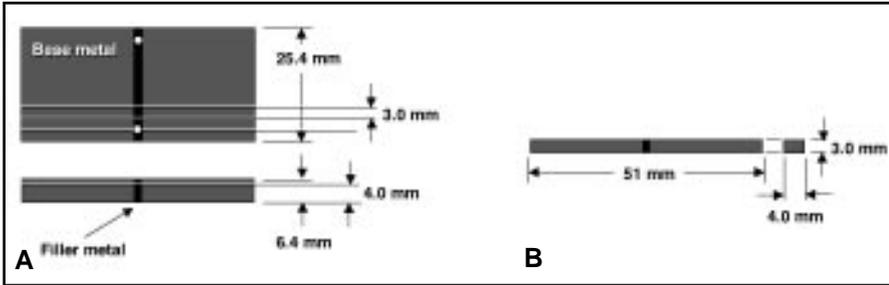$$\theta = tan{-1}[2rh/(r2-h2)] \quad (2)$$

Fig. 4 — A — Schematic diagram showing fabrication of test pieces from the brazed parent blocks; B — dimensions of the four-point bend bars used in the mechanical tests corresponding to MIL-STD-1942A, Type B geometry.
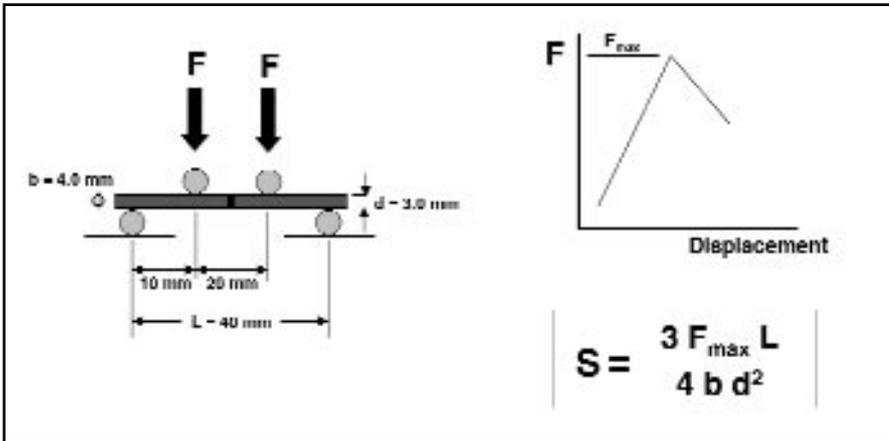

Fig. 5 — Schematic diagram of the four-point bend test per MIL-STD-1942A. The flexure strength, S, was computed from the maximum force, F_{max}

Table 2 — Sessile Drop Contact Angle Per the Peak Brazing Temperature (± 1 standard deviation)

		Contact Angle Values (°)		
			Au-Ni-Ti	
Substrate	Material	1000°C	1033°C	1053°C
Material	Condition	(1832°F)	(1891°F)	(1927°F)
Thermo-Span™	Solution treated	—	—	—
Thermo-Span	Solution treated and aged	5.7 (0.2)	0.5 (1.5)	0.3
347 stainless steel	As-received	5.6 (4.0)	3.5 (1.4)	3.0

The values of the contact angles for each base metal and brazing process are listed in Table 2. In some cases, replicate samples were evaluated to determine the scatter in these measurements. The data in Table 2 shows the contact angles were very low, indicating excellent wetting and spreading by the braze alloys on the substrate materials. The scatter numbers indicated Au-Ni-Ti filler metal performance was relatively insensitive to the brazing temperature range of 1000 to 1053°C (1832 to 1927°F) for a nominal brazing time of 3 min.

The selected brazing process for the Au-Ni-Ti filler metal is illustrated in Fig. 3. Each cycle began with a temperature rise of 10°C/min (18°F/min), to a subsolidus temperature of 900°C (1652°F). A hold time of 5 min allowed the specimen and fixturing to reach an equilibrium temperature. The temperature was then raised at 5°C/min (9°F/min) to the brazing temperature of 1000°C (1832°F) for 7 min. A reduced brazing temperature and longer brazing time (vis-à-vis the wetting experiments) were used to ensure a more repeatable brazing cycle. The specimen temperature was ramped down at 5°C/min (9°F/min) through the solidus point, to the previous holding temperature of 900°C (1652°F). This controlled cooling step duplicated a brazing process for metal-ceramic joints that minimizes the buildup of residual stresses caused by thermal expansion mismatch across the joint. The cooling rate was then increased to 10°C/min (18°F/min) until a temperature of approximately 400°C (752°F) was reached, after which the assembly was allowed to furnace cool to room temperature.

The brazing cycle potentially placed the Thermo-Span alloy back into a solutionized condition. The base metal would require a precipitation aging treatment after the brazing process to obtain the desired properties. This circumstance illustrates the need to understand aging processes in brazed joints and their potential impact on joint performance.

Microstructural Analysis of Sessile Drop Samples

Sessile drop samples were used in some assessments of the interface reactions in the aged couples. The aged samples were evaluated using optical microscopy, scanning electron microscopy (SEM), and electron microprobe analysis (EMPA) techniques.

Mechanical Test Specimen Fabrication

Mechanical strength measurements were performed on individual specimens cut from brazed parent blocks. Shown in Fig. 4A is a schematic diagram illustrating the manner in which tests specimens were cut from brazed blocks. The cuts produced seven test pieces having a width ground to a dimension of 3.0 mm (0.12 in.). Only those five pieces originating from the center portion of the block assembly were used to avoid the tungsten spacer wire. The final dimensions of the test specimens (Fig. 4B) were reached by a grinding operation that reduced the original "thickness dimension" from 6.4 mm (0.25 in.) to 4.0 mm (0.16 in.). Sample geometry complied with MIL-STD-1942A, "Flexure Strength of High Performance Ceramics at Ambient Temperature." Four of the five test samples were used for mechanical tests. The remaining sample was cross sectioned and its microstructure analyzed to supplement data obtained from the sessile drop samples.

Four-Point Bend Mechanical Strength Test Procedure

The four-point bend test setup (per MIL-STD-1942A) is shown in Fig. 5. The test specimen was placed on top of two outer support rollers separated by a distance of 40 mm; the ground surface was in contact with the rollers. The two inner or "loading" rollers separated by a distance of 20 mm (0.79 in.) were positioned on top of the specimen. No significant preload was applied prior to the start of testing.
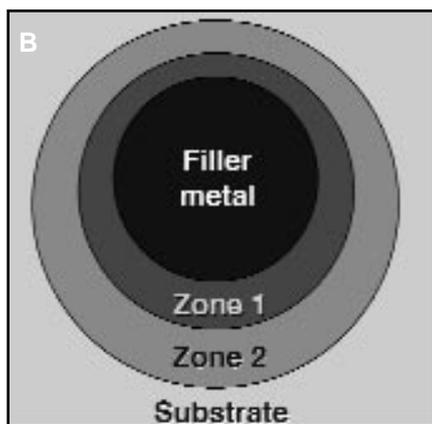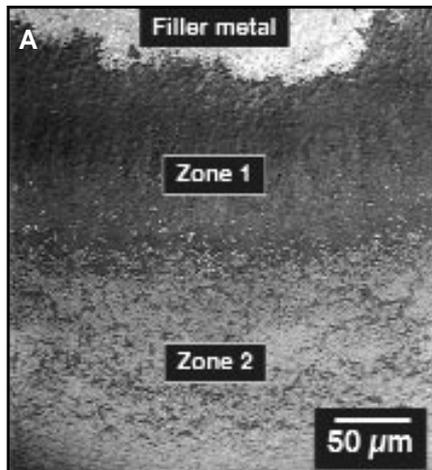
Fig. 6 — A — SEM micrograph of the Au-Ni-Ti sessile drop on the Thermo-Span alloy showing the precursor film structure; B — schematic diagram of the precursor film formed by the spreading Au-Ni-Ti filler metal.
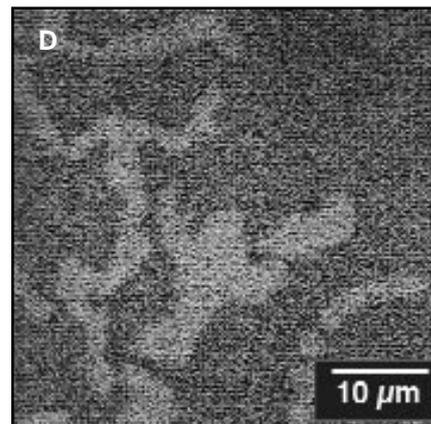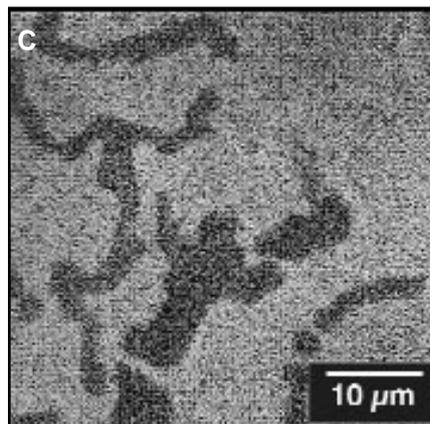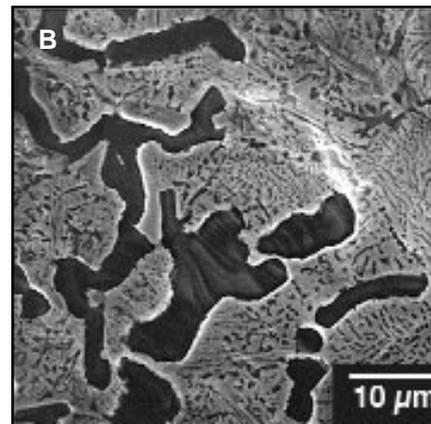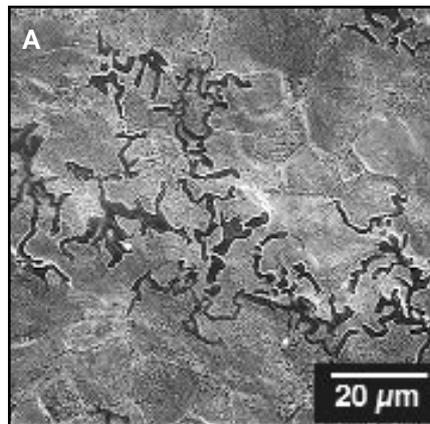

Fig. 7 — A — Low-magnification SEM micrograph of zone 1 of the precursor film from a Au-Ni-Ti sessile drop on the Thermo-Span base metal; B — high-magnification SEM micrograph of zone 1; C — nickel X-ray dot map of the precursor film surface shown in Fig. B; D — gold X-ray dot map of the film area in Fig. B.
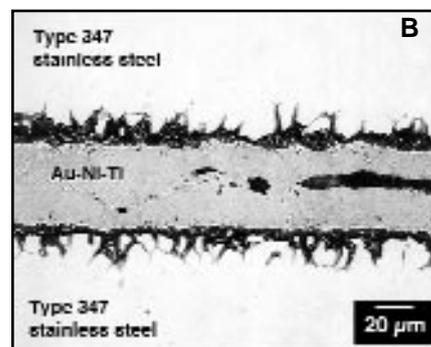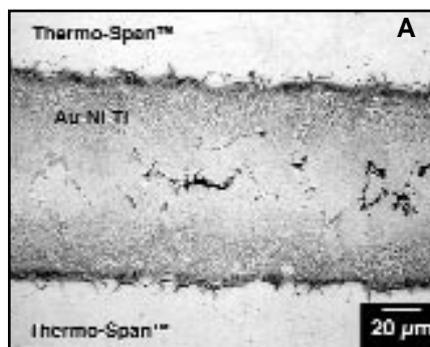
The specimen was subjected to a constant cross head displacement rate of 8.3×10^{-3} mm/s (3.3×10^{-4} in./s). The flexure strength, S, was computed according to the following equation:

$$S = \frac{3\,F_{max}\,L}{4\,b\,d2} \qquad (3)$$

where F_{max} is the maximum force (load); L is a support roller span of 40 mm (1.6 in.); b is the specimen width of 4.0 mm (0.16 in.); and d is the specimen thickness of 3.0 mm (0.12 in.). Strength data were represented by the mean and standard deviation of the multiple tests.

Aging Environments

The aging treatments were performed at temperatures of 225°C (437°F), 460°C (860°F), and 700°C (1292°F), and time periods of 100, 200, and 300 days. Each specimen was placed in a quartz ampoule along with a piece of Ta foil. The ampoule was then backfilled with Ar at a 10-mtorr (1.3-Pa) pressure and sealed. The Ta foil served as a getter for residual oxygen.

Fig. 8 — Optical micrographs showing cross sections of A — The Thermo-Span ; B — the 347 stainless steel, four-point bend joints made with the Au-Ni-Ti filler metal. The Thermo-Span sample was etched in a $H_2O/HCl/HNO_3/CrO_3$ solution. The Type 347 stainless steel sample was etched in Villela's solution followed by a $FeCl_3$ solution.

Sessile drop specimens were fabricated to evaluate microstructural changes due to these aging treatments. A more limited range of aging parameters was used for the four-point bend samples due to material availability; those parameters were 460°C (860°F) and 700°C(1292°F) and the time periods were 87 and 200 days.
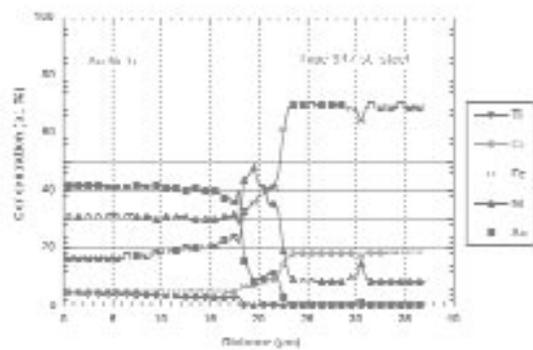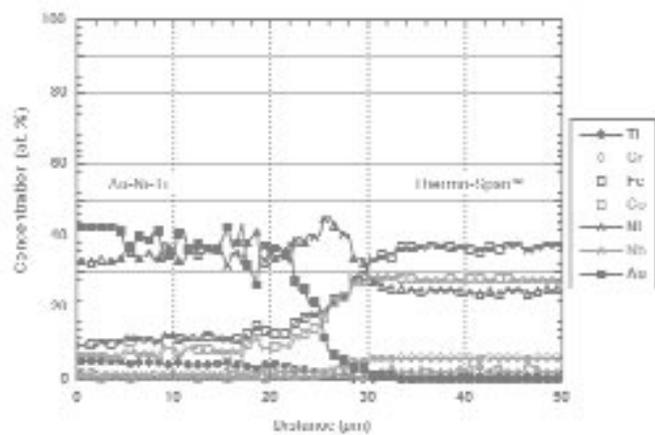
Results and Discussion

Sessile Drop Morphology from the Wetting and Spreading Experiments

An SEM micrograph of the leading edge of the Au-Ni-Ti sessile drop on Thermo-Span resulting from the brazing
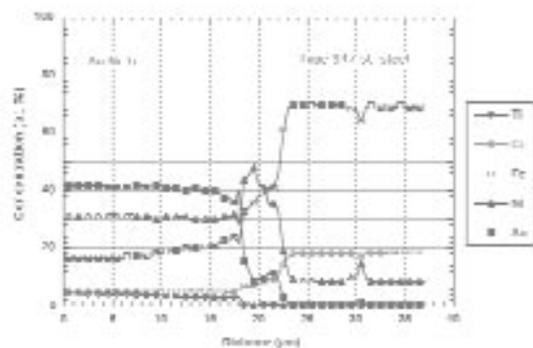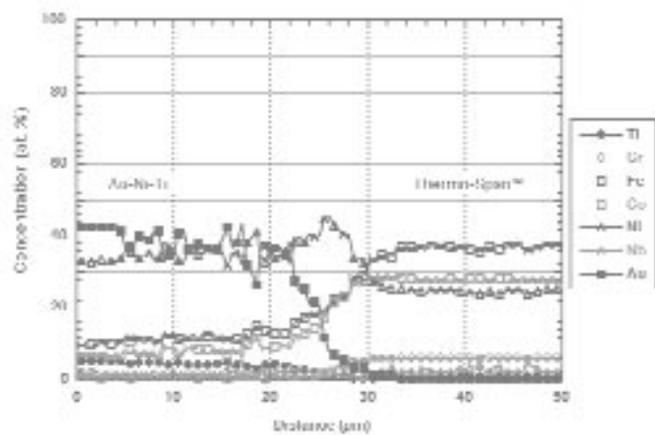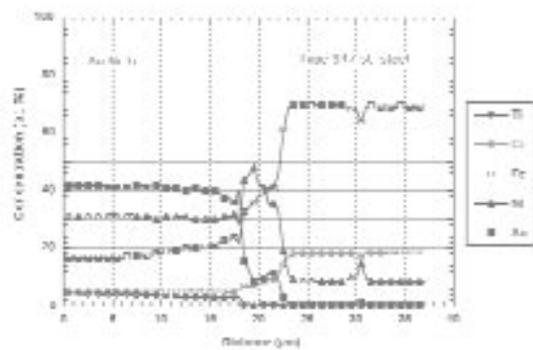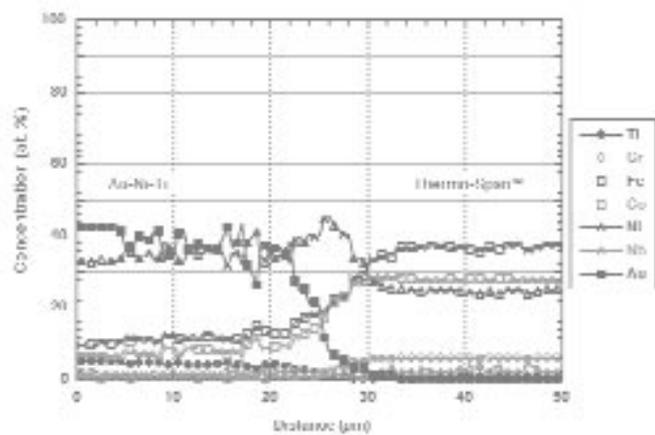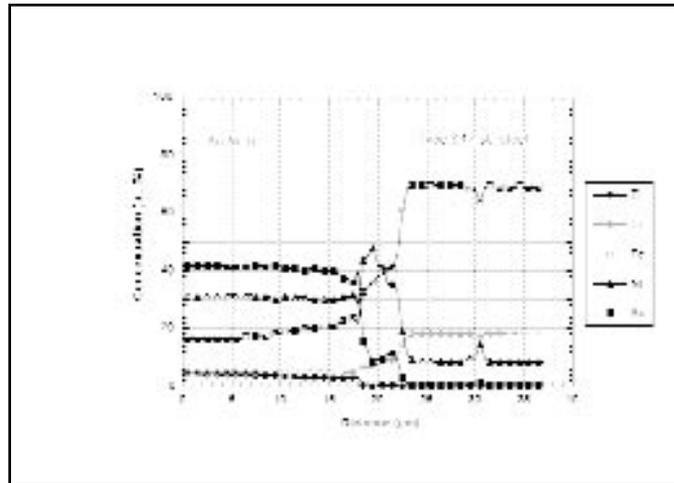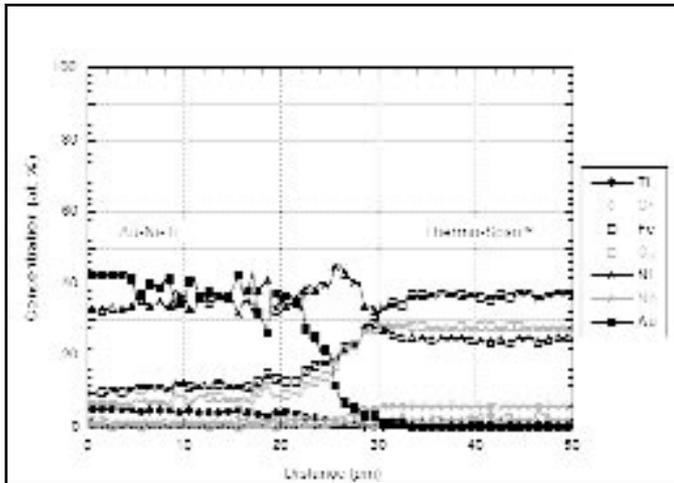
Fig. 9 — Representative EMPA trace of the interface region between Au-Ni-Ti filler metal and Thermo-Span base metal in the as-fabricated condition.

Fig. 10 — Representative EMPA trace of the interface region between Au-Ni-Ti filler metal and Type 347 stainless steel base metal in the as-fabricated condition.
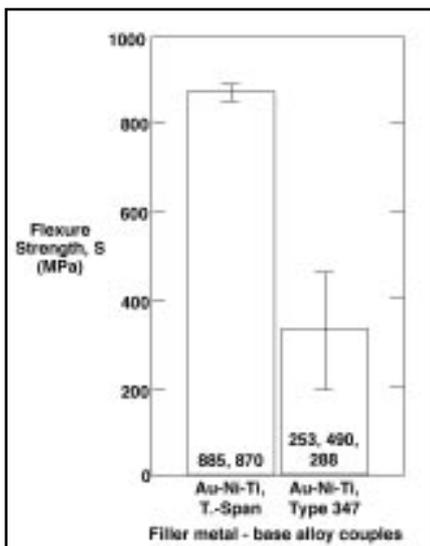

Fig. 11 — Four-point bend strengths of the as-fabricated joints made with Thermo-Span and Type 347 stainless steel base metals. The length of the bars equal the data mean; the individual test values are included within each bar.
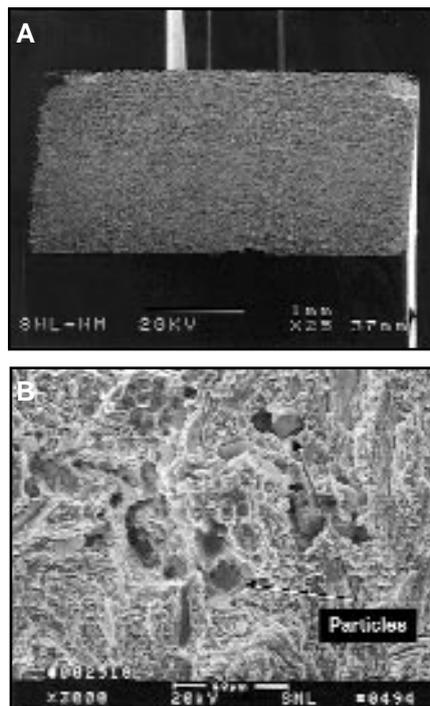

Fig. 12 — A — Low-magnification SEM photograph of the fracture surface of a Thermo-Span base metal/Au-Ni-Ti filler metal joint tested in the as-fabricated condition; B — a high-magnification SEM photograph of the same.

conditions of 1053°C (1927°F) and 7 min appears in Fig. 6A. A schematic diagram of the Au-Ni-Ti sessile drop surface morphology appears in Fig. 6B. Three distinct regions were observed: the bulk filler metal as well as "zone 1" and "zone 2" of a precursor film. Low- and high-magnification SEM micrographs of zone 1 appear in Figs. 7A and 7B, respectively. Energy-dispersive X-ray analysis (EDXA) maps of nickel and gold are shown in Figs. 7C and 7D, respectively, for the area in Fig. 7B. The EDXA determined zone 1 to be comprised of nickel-rich islands in a matrix of gold-rich phase. There was no significant-titanium signal. The EDXA also detected the presence of iron, silicon, and chromium, which suggested some dissolu-

tion of the underlying Thermo-Span substrate material had taken place.

The morphology of zone 2 was similar to that of zone 1 with the exception that the segregation of the nickel and gold constituents into nickel-rich islands in a gold-rich matrix was less distinct. Analysis did not reveal the presence of titanium.

The same evaluation was made of the wetting and spreading behavior by the Au-Ni-Ti filler metal over the Type 347 stainless steel. The same brazing conditions

were used. A two-zone precursor film morphology was observed, having the same gold and nickel elemental distributions as were identified with the Thermo-Span base metal.

Brazed Joint Microstructure — As-Fabricated Condition

The brazed joint microstructures that formed between the Au-Ni-Ti filler metal and the Thermo-Span and Type 347 stainless steel base metals were examined through observations of cross sections. Representative micrographs of the as-fabricated Thermo-Span/Au-Ni-Ti and Type 347 stainless steel/Au-Ni-Ti joints are shown in Figs. 8A and 8B, respectively. The Thermo-Span joints (Fig. 8A) exhibited reaction zones at the filler metal/base metal interfaces. Such reaction zones were not apparent in the Type 347 stainless steel/Au-Ni-Ti couples. Grain boundary infiltration and dissolution were observed in the base metals along the interface, going to a depth of approximately ½ to 1 grain for the Thermo-Span material and 1 to 2 grains deep in the Type 347 stainless steel.

Figure 9 shows a representative electron microprobe analysis (EMPA) trace that was taken across the Thermo-Span base metal/Au-Ni-Ti filler metal interface. No intermetallic compound layers were identified. Rather, a compositional transition zone was observed that ranged from 15 μm to approximately 35 μm wide. A concentration maximum of Ni was observed. There was no preferential concentration of titanium within the zone. Concentration gradients of iron and cobalt, and to a lesser degree niobium and chromium, indicated base metal dissolution and some liquid-state diffusion were active during the brazing process. There

were significant concentrations of iron (10 at.-%) and cobalt (7 at.-%) and trace amounts of chromium and niobium in the filler metal away from the interface; the titanium, gold, and nickel concentrations there were commensurate with the nominal composition of the filler metal.

Electron microprobe analysis was performed across the interface between the Au-Ni-Ti filler metal and the Type 347 stainless steel base metal. A representative EMPA trace is shown in Fig. 10. A transition zone was observed between the filler metal and the base metal. In Fig. 10, that zone was approximately 8 μm wide, but was as wide as 15 to 30 μm at some locations. As in the case of the Thermo-Span alloy, a similar Ni concentration peak was observed in that zone. Titanium was not present at significant levels in the transition zone.

Elevated concentrations of iron (17 at.-%) and chromium (4 at.-%) were observed in the filler metal. A comparison was made of the EMPA trace in Fig. 10 with that of the Thermo-Span/Au-Ni-Ti couple in Fig. 9. A higher iron concentration was observed in the remaining filler metal of the Type 347/Au-Ni-Ti couples. The greater iron levels in the latter couples was likely due to the higher Fe concentration in that base metal.

A few isolated voids were observed in the filler metal. Those voids did not have a morphology that indicated poor wetting of the base alloy surfaces. Rather, possible causes included, individually or in combination: 1) outgassing by the base metals and/or filler metal at the elevated temperatures; 2) insufficient filler metal quantity to keep the joint clearance filled under the extensive interface reactions; and 3) solidification shrinkage.

Four-Point Bending Strength — As-Fabricated Condition

Four-point bend strengths are shown in Fig. 11 for the as-fabricated joints made with Thermo-Span and the AISI Type 347 stainless steel base metals using the Au-Ni-Ti filler metal. The Thermo-Span joints exhibited the highest strengths at a mean value of 880 MPa (128 ksi). In fact, some deformation of Thermo-Span base metal was observed that may have resulted from partial solution annealing during the brazing cycle. On the other hand, the Type 347 stainless steel joints had relatively low strength of 340±139 MPa (49±20 ksi).

Cross sections of post-tested Thermo-Span and Type 347 stainless steel braze joints indicated the fracture paths of both specimen types were in the filler metal. A low-magnification SEM image of the Thermo-Span specimen fracture surface is shown in Fig. 12A. A 3000X magnification image of the fracture surface in Fig. 12B shows extensive deformation in the material at this scale. Within that deformation, individual particles were also observed. Similar low- and high-magnification SEM images of the fracture surface of a Au-Ni-Ti filler metal/Type 347 stainless steel base metal joint are shown in Fig. 13. The 3000X magnification view in Fig. 13B distinguished a faceted appearance to the fracture surface indicative of an intergranular failure mode. The facet size was approximately 1 to 2 μm (3.9 x 10^{-5} in. to 7.8 x 10^{-5} in.). Therefore, an intergranular failure mode may have been responsible for the reduced strength of the brazed joints made to the Type 347 stainless steel base metal. A possible source of this failure mode was the elevated concentrations of iron and chromium found in the filler metal in these joints.

Brazed Joint Microstructure — Post-Aging Condition

Small changes in the braze joint microstructure were observed for couples formed between the Thermo-Span base metal and Au-Ni-Ti filler metal after aging
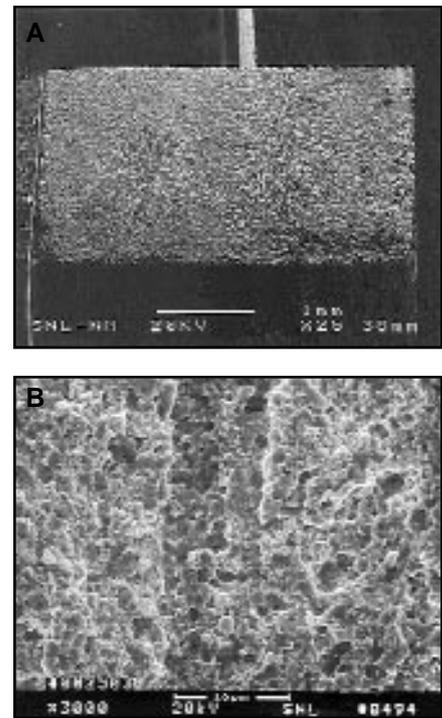
Fig. 13 — A — Low-magnification SEM photograph of the fracture surface of a Type 347 stainless steel base metal/Au-Ni-Ti filler metal joint tested in the as-fabricated condition; B — a high-magnification photograph of the same.

at 225°C (437°F) or 460°C (860°F). The interface reaction zone retained a high concentration of nickel. There was no development of intermetallic compounds. The filler metal microstructure likewise remained unchanged from that observed in the as-fabricated specimens.

Joint microstructure did change in specimens exposed to a 700°C (1292°F) aging temperature. Shown in Fig. 14A is a low-magnification micrograph of the Thermo-Span/Au-Ni-Ti joint after aging for 437 days. Two distinct morphologies were observed: a lighter area was located
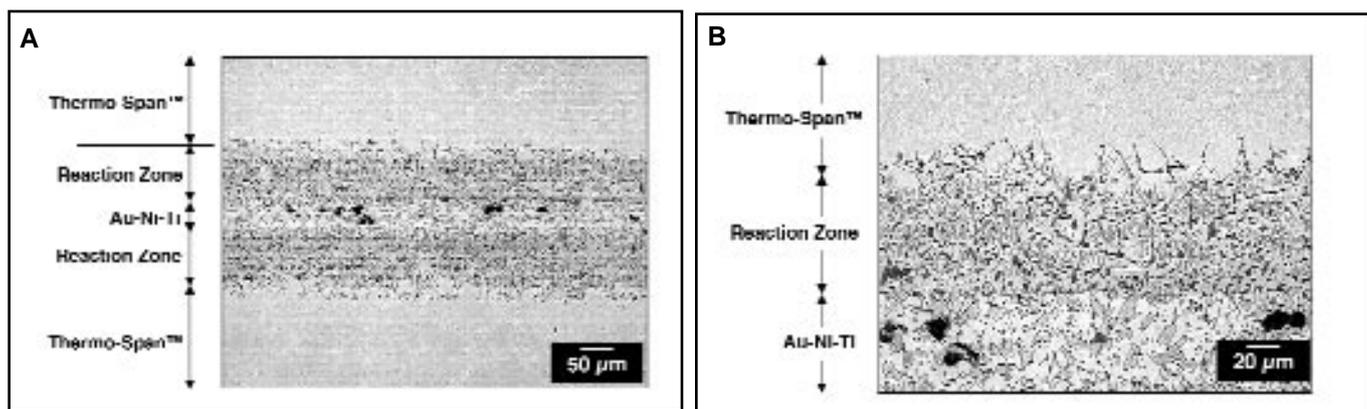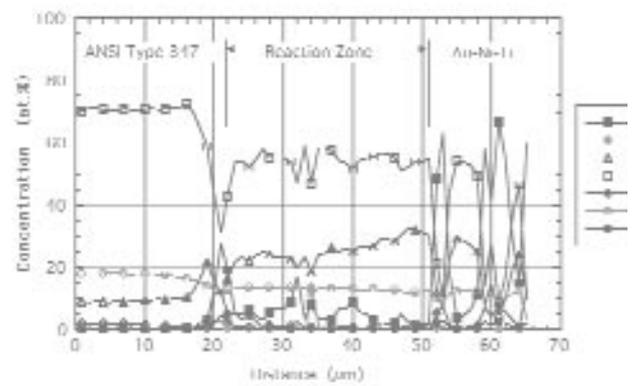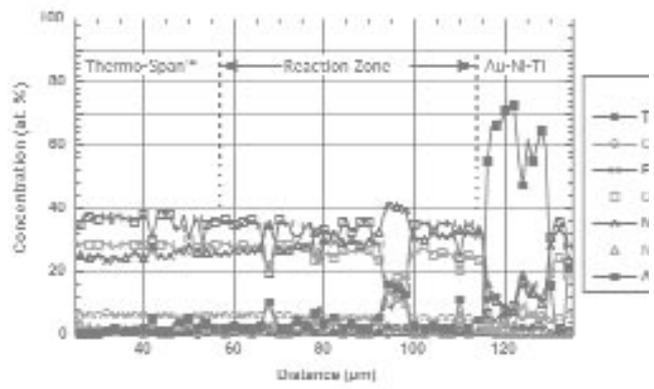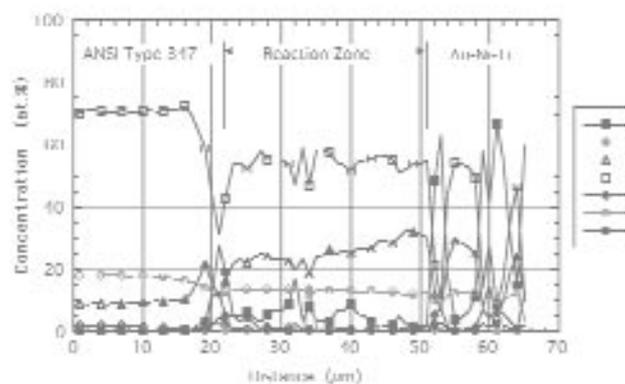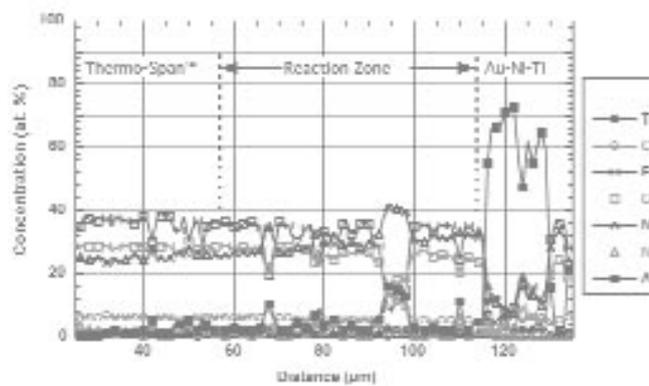
Fig. 14 — A — Low-magnification, optical micrograph of a Thermo-Span/Au-Ni-Ti joint after aging at 700°C (1292°F) for 437 days. The base metal, reaction zones, and filler metal have been identified; B — a high-magnification, optical micrograph of the reaction zone formed between the base alloy and filler metal.

Concentration (at.%)

Thermo-Span® ←— Reaction Zone —→ Au-Ni-Ti

100
80
60
40
20
0

40   60   80   100   120

Distance (μm)

ANSI Type 347   Reaction Zone   Au-Ni-Ti

Concentration (at.%)

100
80
60
40
20
0

0   10   20   30   40   50   60   70

Distance (μm)
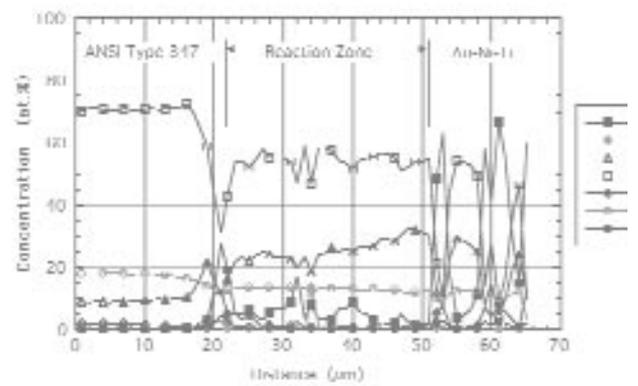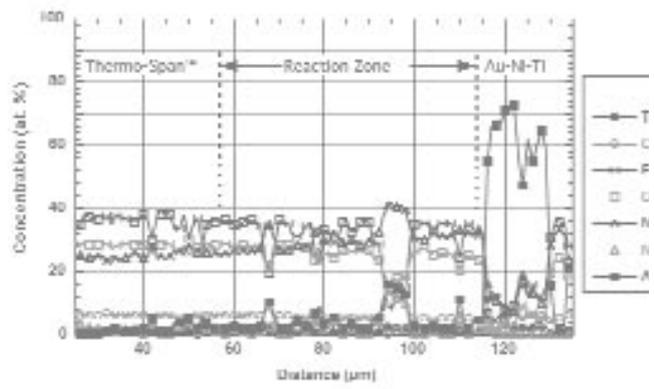
Fig. 15 — Electron microprobe analysis trace across the reaction zone formed between Thermo-Span base metal and the Au-Ni-Ti filler metal after aging at 700°C (1292°F) for 437 days.

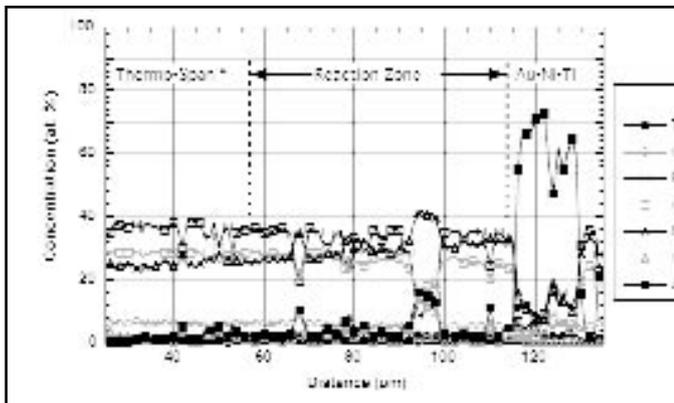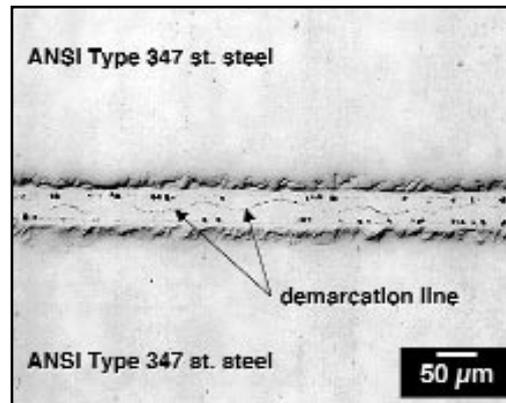*Fig. 16 — An optical micrograph (differential interference contrast) taken of a Type 347 stainless steel/Au-Ni-Ti sample aged at 225°C (437°F) for 300 days. The demarcation line in the filler metal has been noted.*
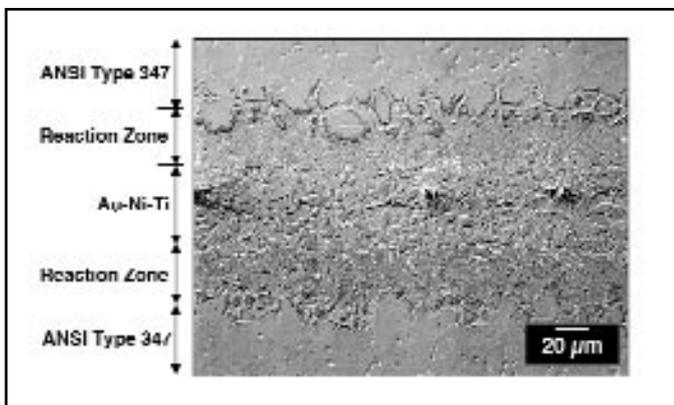

Fig. 17 — An optical micrograph (differential interference contrast) taken of the Type 347 stainless steel/Au-Ni-Ti sample aged at 700°C (1292°F) for 437 days. The Au-Ni-Ti filler metal, reaction zones, and Type 347 stainless steel base metal regions have been noted.
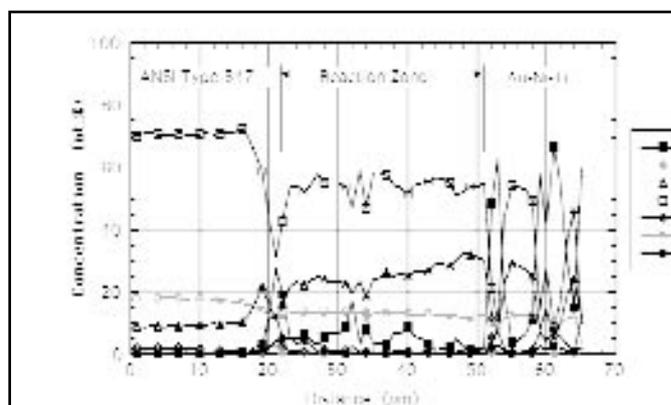

Fig. 18 — Electron microprobe analysis trace across a Type 347 stainless steel/Au-Ni-Ti braze joint aged at 700°C (1292°F) for 437 days.

at the center of the joint with a width of approximately 55 μm (0.0021 in.), and two reaction layers of darker contrast were located to either side of the center region and had thicknesses of 60 to 80 μm (0.0023 to 0.0031 in.). A comparison of this aged microstructure with that of the as-fabricated specimen (Fig. 8A) indicated the aging treatment caused 1) changes to the filler metal and interface reaction zone microstructures and 2) enlargement of the interfacial reaction zones by a factor of two to three. The high magnification micrograph in Fig. 14B suggests significant phase formation had taken place along Thermo-Span grain boundaries as well as within the grains themselves.

The chemical composition of the Thermo-Span/Au-Ni-Ti reaction zone and neighboring Thermo-Span base metal were identified by EMPA — Fig. 15. A grain boundary phase, which formed in the nearby Thermo-Span base material, was examined first. Unaged Thermo-Span alloy exhibited an enrichment of niobium

and cobalt as well as reduced levels of nickel, iron, and chromium at the grain boundaries. In the case of aged Thermo-Span/Au-Ni-Ti couples, the Thermo-Span grain boundaries exhibited a further increase in the niobium concentration; however, the cobalt concentration decreased there. In addition, the grain boundaries showed significant concentrations of gold and nickel, as well as the appearance of a small titanium concentration. Concurrently, the iron and chromium concentrations dropped below their nominal values for the bulk Thermo-Span base metal. When nickel content was adjusted for its nominal concentration in the base metal, the grain boundary showed a composition of 78Au-21Ni-1Ti (wt-%) plus Nb. The Au-Ni-Ti combination was very similar to the nominal composition of the filler metal (81Au-17.5Ni-1.5Ti, wt-%). This analysis suggests the 700°C (1292°F), 437 day aging condition allowed solid-state diffusion of the filler metal elements gold, nickel, and titanium along the Thermo-

Span grain boundaries such that the filler metal composition was essentially reproduced at the expense of iron, cobalt, and chromium.

Recall the as-fabricated Thermo-Span/Au-Ni-Ti joints exhibited a reaction zone having a relatively smooth concentration gradient of gold, nickel, iron, and other elements between the base and filler metal (see Fig. 9). Aging appears to have caused a noticeable segregation of elements. First, at the boundary between the reaction zone and the (nominal) Au-Ni-Ti filler metal, a gold concentration increase was observed. Second, the filler metal contained a matrix phase and a particle phase. The matrix phase had the following composition: gold (67 at.-%), titanium (15 at.-%), nickel (12 at.-%), iron (3 at.-%), cobalt (2 at.-%), and chromium (1 at.-%). The particle phase had the reproducible (± 1 at.-%) composition of iron (36 at.-%), nickel (33 at.-%), cobalt (24 at.-%), chromium (5 at.-%), and gold (1–2 at.-%). Binary phase diagrams of the Cr-
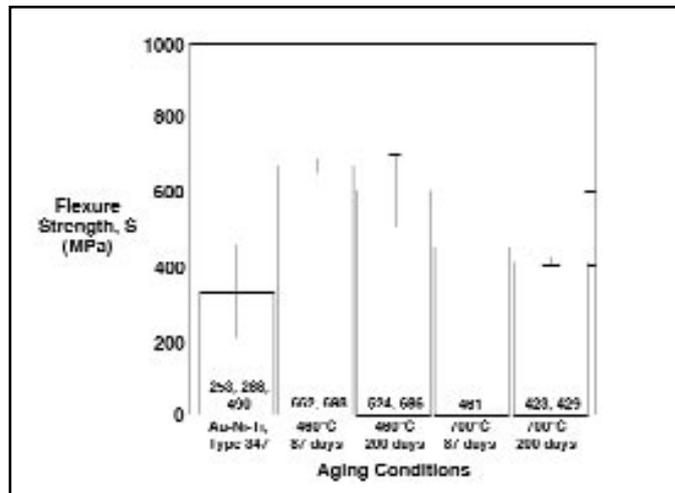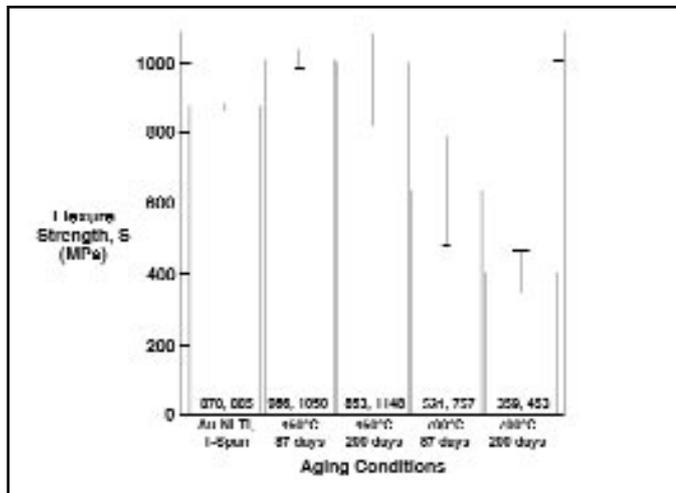
Fig. 19 — Bar chart showing the four-point bend strength of the Thermo-Span/Au-Ni-Ti joints after aging.

Fig. 21 — Bar chart showing the four-point bend strength of the Type 347 stainless steel/Au-Ni-Ti joints after aging.

Fe, Cr-Ni, and Fe-Ni alloy systems exhibit extensive regions of mutual solubility, of course when fully liquid, but also when solid at high temperatures. However, those high-temperature solid solutions generally decompose by phase separation at lower temperatures. A similar scenario was hypothesized to have occurred in the braze joint. That is, aging caused phase separation of the filler metal, which now included dissolved base metal components, into the matrix and particle phases discussed above. That scenario appeared to be more likely than the formation of two phases by long-range, solid-state diffusion of the Thermo-Span base metal constituents during the aging treatment.

The aged braze joints made between the Type 347 stainless steel base metal and Au-Ni-Ti filler metal were similarly examined. The braze joint area, including the filler metal and the reaction zones, did not grow significantly after aging for up to 300 days at either 225°C (437°F) or 460°C (860°F). However, an artifact that was associated with these aging conditions was a demarcation line down the center of the joint. This artifact is shown by the optical micrograph in Fig. 16 of a specimen aged at 225°C (437°F) for 300 days. Electron microprobe analysis determined the line to be rich in nickel and titanium. Gold and iron were also present as was a trace of chromium. A specific composition of the line could not be determined due to its thin stature.

An appreciable increase in size of the braze joint was observed for Type 347 stainless steel/Au-Ni-Ti couples aged at 700°C (1292°F). This point is illustrated by the optical micrograph in Fig. 17 of the specimen aged for 437 days. A reaction zone approximately 35 μm (0.0014 in.) developed at the base metal/filler metal interface. Because the Au-Ni-Ti filler metal region exhibited a thickness similar to that in the as-fabricated case, the reaction zones formed along the stainless steel grain boundaries and then developed further into the base metal by subsequent "consumption" of the base metal grain.

A representative EMPA trace made across the braze joint is shown in Fig. 18. At the interface between the stainless steel and reaction zone, gold and titanium peaks were accompanied by a minimum in the Fe concentration. Progressing through the reaction zone, from the stainless steel to the filler metal, the following trends were noted: iron, chromium, manganese, and titanium concentrations remained relatively constant at 54 at.-%, 13 at.-%, <1 at.-%, and 0 at.-%, respectively. An increase in nickel concentration from 22 to 30 at.-%, and a decrease in the gold concentration from 6 to 1 at.-% was observed.

The Au-Ni-Ti filler metal was comprised of two phases, a matrix phase and a particle phase (which, again, was not present in the as-fabricated joint). The matrix phase contained from 8 to 10 at.-% of each of the following elements: iron, nickel, manganese, and chromium as well as 2 at.-% of titanium; the remaining content was gold. The gold/nickel ratio was much higher after aging than was its value in the as-fabricated joint. The particle phase had a composition of iron (55 at.-%), nickel (30 at.-%), chromium (13 at.-%), and gold (2 at.-%). Aside from the presence and/or absence of particular elements per the respective base metal compositions, differences in the matrix and particle phase compositions between these Au-Ni-Ti/Type 347
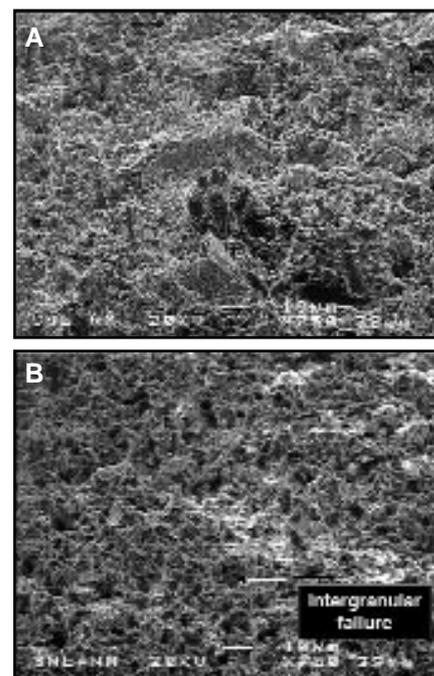

Fig. 20 — SEM photographs of the fracture surfaces of Thermo-Span/Au-Ni-Ti, four-point bend joints specimens. A — In the as-fabricated condition; B — following aging at 700°C (1292°F) for 200 days.

stainless steel couples and similarly aged Au-Ni-Ti/Thermo-Span couples reflected primarily the different compositions of the respective base metals. As was hypothesized in the analysis of the latter couples, the particle phase formed during the aging treatment by precipitation of compounds comprised of elements dissolved in the filler metal at the time the joint was formed.

Four-Point Bending Strength — Post Aging

Shown in Fig. 19 is a bar chart depicting the four-point bend strength of Thermo-Span/Au-Ni-Ti joints after aging. The bend strength increased from a mean value of 880 MPa (128 ksi) for the as-brazed joints to mean values of 1020 MPa (148 ksi) and 1000 MPa (145 ksi) after aging at 460°C (860°F) for 87 and 200 days, respectively. The joint strengths then decreased to values of 600 MPa (87.1 ksi) and 410 MPa (59.5 ksi) when aged at 700°C (1292°F) for the same respective time periods. Scanning electron microscopy of the fracture surfaces together with optical microscopy and EMPA evaluations of fracture surface cross sections showed failure within the filler metal for the high-strength specimens aged at 460°C (860°F).

The strength decrease for Thermo-Span/Au-Ni-Ti couples after aging at 700°C (1292°F) was accompanied by the two previously described microstructural changes: 1) the development of a reaction zone at the Thermo-Span/Au-Ni-Ti interface and 2) the precipitation of a particle phase in the remaining filler metal. Shown in Fig. 20A is a SEM photograph of the fracture surface representing the as-fabricated condition. (Note the magnification is significantly lower than that of Fig. 12B.) Shown in Fig. 20B is the fracture surface of the specimen tested after aging at 700°C (1292°F) for 200 days. The larger scale of deformation associated with the as-fabricated sample was replaced by mixture of smaller scale deformation surrounding particles for the aged sample. The latter fracture surface morphology is consistent with particle precipitation in the filler metal.

In summary, the effect of aging on the four-point strengths of Thermo-Span/Au-Ni-Ti couples reflected a precipitation strengthening mechanism based upon particles comprised of base metal elements dissolved in the filler metal at the time of brazing. The strengthening was maximized when aging at 460°C (860°F) as the formation of nanometer space particles took place. However, aging at 700°C (1292°F) resulted in an over-aging condition. The particles grew significantly larger, now being visible in cross section and on the SEM fracture surface — Fig. 20. Concurrent with particle enlargement was a drop in joint strength.

The strength behavior of Type 347 stainless steel/Au-Ni-Ti joints as a function of aging is shown in Fig. 21. The strength of the as-fabricated specimens was 340 MPa (49.3 ksi). Aging at 460°C (860°C) caused an increase in strength to 680 MPa (98.7 ksi) and 605 MPa (87.8 ksi) for time periods of 87 and 200 days, respectively. However, aging at 700°C (1292°F) resulted in a strength decrease to 461 MPa (66.9 ksi) after 87 days and 426 MPa (61.8 ksi) after 200 days. This dependence of joint strength on aging was very similar to the Thermo-Span/Au-Ni-Ti couples. That similarity also extended to the fracture surface morphologies (Fig. 20), as determined by SEM analysis.

Summary

1) The effects of aging on microstructure and bend strength were examined for brazed joints made with 81Au-17.5Ni-1.5Ti filler metal and either Thermo-Span or AISI Type 347 stainless steel base metals.

2) Excellent wetting and spreading were exhibited by the Au-Ni-Ti filler metal on both base metal surfaces.

3) Sessile drop morphology showed a two-zone precursor structure at the edge of the spreading Au-Ni-Ti filler metal.

4) A 15- to 35-μm-wide reaction zone formed at the interface between the Thermo-Span alloy and Au-Ni-Ti filler metal in the as-fabricated joints. Aging at 700°C (1292°F) caused the reaction zone to grow; however, the mechanical strength behavior of the joints was not affected by the zone.

5) Significant quantities of iron (10 at.-%) and cobalt (7 at.-%), and trace amounts of chromium and niobium, were identified in the filler metal area of the as-fabricated Thermo-Span joints. Aging at 700°C (1292°F) caused the precipitation of particles in the filler metal area, which had the following composition: Fe (36 at.-%), Ni (33 at.-%), Co (24 at.-%), Cr (5 at.-%), and Au (1–2 at.-%). The precipitates originated from base metal elements that dissolved into the filler metal at the time the braze joint was made.

6) Type 347 stainless steel/Au-Ni-Ti joints exhibited similar microstructural features in the as-fabricated condition, as well as changes to those features after aging, as were observed with the Thermo-Span base metal. The compositions of the interface reaction zone and particles that precipitated in the filler metal area after aging reflected the particular composition of the stainless steel base metal.

7) The effect of aging on the four-point bend strengths of the Thermo-Span/Au-Ni-Ti and AISI Type 347 stainless steel couples indicated a precipitation strengthening mechanism. Specifically, strengthening was observed by aging at 460°C (860°F). An over-aging condition resulted from heat treating at 700°C (1292°F) as indicated by a drop in bend strength.

References

1. Mangin, C., Neely, J., and Clark, J. 1993. The potential for advanced ceramics in automotive engine applications. *Journal of Metals* June: 23–27.

2. DeLuca, M., and Swain, J. 1987. An advanced ceramic-to-metal joining process. *Ceram. Eng. Sci. Proc.* 8[7-8]: 602–610.

3. Santella, M. 1993. Joining of ceramics for heat engine applications. *Ceramic Tech. Project-Semiannual Prog. Rep. For Oct. 1992–March 1993,* ORNL/TM-12428: 167–180.

4. Bex, W. 1989. Metallurgical study of superalloy brazing alloys. *Proc. Propulsion and Energetics panel at the 72nd Specialists' Meeting,* Bath, UK.3-5 Oct.: pp. 27-1 to 27-12.

5. Sasabe, K. 1991. Effect of joint clearance on fatigue strength of brazed joint. *Trans. Nat. Res. Inst. For Metals* 33(1), pp. 36–41.

6. Dicus, D., and Buckley, J. 1972 The effects of high-temperature brazing and thermal cycling on the mechanical properties of Hastelloy X. *NASA Langley Research Center Report:* L-8376, pp. 1–21.

7. Shimoo, T., Kobayashi, Y., and Okamura, K. 1992. Kinetics of reaction of Si_3N_4 with Ni. *Jour. of the Cer. Soc. of Japan,* Inter. Edition 100, pp. 801–806.

8. Naka, M. 1992. Controlling of ceramic-metal interfacial structure using molten metals. *Trans. Weld. Res. Inst.* 21: 1–7.

9. Boadi, J., Yano, T. and Iseki, T. 1987. Brazing of pressureless-sintered SiC using Ag-Cu-Ti alloy. *Jour. of Mater. Sci.* 22: 2431–2434.

10. Bang, K., and Liu, S. 1994. Interfacial reaction between alumina and Cu-Ti filler metal during reactive metal brazing. *Welding Journal* 73:54-s to 60-s.

11. Thermo-Span is a registered trademark of Carpenter Technologies Corp.

12. Wilbraze™ is a registered trademark of the former Wilkinson Corp.